PROCEEDINGS OF THE FIFTEENTH SYMPOSIUM ON ELECTROMAGNETIC WINDOWS

June 18–20, 1980

Edited by
H. L. Bassett
and
G. K. Huddleston

GEORGIA INSTITUTE OF TECHNOLOGY
ATLANTA, GEORGIA 30332

PROCEEDINGS OF THE FIFTEENTH SYMPOSIUM ON ELECTROMAGNETIC WINDOWS

June 18—20, 1980

Edited by
H. L. Bassett
and
G. K. Huddleston

GEORGIA INSTITUTE OF TECHNOLOGY
ATLANTA, GEORGIA 30332

FOREWORD

The Fifteenth Electromagnetic Window Symposium marks 25 years of regularly scheduled symposia on electromagnetic windows. The first seven symposia were held at Ohio State University. The Georgia Institute of Technology has hosted the symposium biennially since 1966, with the U. S. Air Force cohosting the symposia of 1966, 1968, and 1972.

The Steering Committee responsible for the team planning and coordination of the symposium consisted of the following individuals from the Georgia Institute of Technology:

D. J. Kozakoff, General Chairman
Engineering Experiment Station

H. L. Bassett, Technical Program Chairman
Engineering Experiment Station

J. M. Newton, Registration Chairman
Engineering Experiment Station

G. K. Huddleston, Publications Chairman
School of Electrical Engineering

E. B. Joy, Publicity Chairman
School of Electrical Engineering

J. N. Harris, Local Arrangements Chairman
Engineering Experiment Station

In addition, G. H. Adams and R. V. Eberwein of Continuing Education put forth significant efforts in the coordination of the meeting activities and mailing out of brochures.

Papers not received in time for publication will be available during the meeting from either the registration desk or the particular author.

For the Steering Committee,

G. K. Huddleston

G. K. Huddleston
Proceedings Editor

TABLE OF CONTENTS

TABLE OF CONTENTS (Continued)

TABLE OF CONTENTS (Continued)

TABLE OF CONTENTS (Continued)

EFFECTS OF INCIDENT POLARIZATION ON RADOME-INDUCED BORESIGHT ERRORS

David G. Burks
Antenna Laboratory
Texas Instruments Inc.
Dallas, Texas

Edward R. Graf
Electrical Engineering
Auburn University
Auburn, Alabama

Michael D. Fahey
U.S. Army Missile Command
Redstone Arsenal, Alabama

An analytic technique is presented which demonstrates the sensitivity of radome-induced boresight errors (BSE) to the polarization of the incident field. The approach is based on a ray-tracing procedure to find the incident fields at the antenna and a surface integration to find the receive voltage. The incident fields at the antenna aperture have a polarization dependence due to the polarization properties of the radome wall transmission and reflection coefficients. Examples are given for a tangent ogive radome with a circular aperture antenna gimballed on two axes.

Theory

All formulations for radome problems are based on the Lorentz reciprocity theorem and differ only in the closed surface chosen for integration and approximations made for the antenna fields [1]. In this paper the voltage received by a monopulse aperture antenna is found by an integration of the incident fields over the surface of a circular aperture. In the transmitting mode the antenna is represented by equivalent surface currents. These currents act as weighting functions on the incident field when the receive voltages are computed.

The radome considered here is a tangent ogive with constant wall thickness, as suggested by Figure 1. Inside the radome is an aperture-type monopulse antenna which may be a reflector or a slotted array. The antenna is gimballed on two axes in order to scan to any angle in the forward half-space. The axis of the radome is taken as the y-axis. Points on the radome are given by unprimed coordinates and antenna points are described by primed coordinates as indicated in Figure 1. The aperture is scanned by rotating about the x' axis by angle α and then rotating about the z' axis by angle β.

Monopulse tracking is performed in both the α and β scan directions by using aperture illumination functions that have the appropriate even and odd symmetries about the given scan axes. Various aperture illuminations have been studied but in all cases the difference patterns were taken as the derivative of the sum pattern in the scan direction and equal radiated power from the sum and difference patterns was assumed.

The antenna is circular polarized as could be obtained by placing a polarizer over a slotted array. This configuration was selected so that the antenna would not demonstrate any polarization sensitivity to

linear-polarized fields when operated without the radome.

The incident fields at the antenna are required in order to use the receiving formulation based on integration over the antenna aperture. To find these fields, a well known ray-tracing technique [2] is used. This technique, which is purely optical, has been shown to produce good results for electrically large radomes [3], such as are considered here. Basically, the procedure is to assume the incident field is composed of a bundle of parallel rays. The radome is assumed to be a locally planar slab tangent to the radome at the ray intersection points and a plane-wave transmission coefficient modifies the incident field. The angle of incidence is the angle between the surface normal and the ray. These two vectors define a plane of incidence and the incident field is decomposed into components that are parallel and perpendicular to this plane. The transmitted rays are assumed to remain in a bundle and propagate parallel to the incident rays.

The above procedure may also be used to treat rays that enter the antenna aperture by reflection from the interior radome wall. In this case transmission is handled as before, but when a transmitted ray strikes the interior of the opposite wall it is modified by the wall reflection coefficient and redirected as prescribed by Snell's reflection law. Such reflected rays can have a significant effect on boresight errors at certain scan angles.

The incident field is assumed to be linear polarized and the polarization direction will be defined with respect to the plane formed by the radome axis and the incident ray that passes through the aperture center. Polarization in this plane is defined as transverse magnetic (TM) and polarization perpendicular is transverse electric (TE). Unit vectors in the TE and TM directions are indicated in Figure 1. Arbitrary polarized incident fields can be expressed as the sum of TE and TM components. The polarization angle, γ, shown in Figure 1 is used here to describe the polarization direction.

The receive voltages are given by the reaction integral,

$$V = C\iint \bar{J}_S \cdot \bar{E}^i - \bar{M}_S \cdot \bar{H}^i \, ds \qquad (1)$$

where $\bar{E}^i$ and $\bar{H}^i$ are the incident fields at the aperture, $\bar{J}_S$ and $\bar{M}_S$ the equivalent surface currents for the antenna when transmiting (either sum or difference modes), C is a constant, and the integration is performed over the aperture.

Boresight errors are computed by positioning the aperture normal to the incident field and computing the monopulse indicated angle, ϵ, given by

$$\epsilon = K^{-1} \, \mathrm{Re}\left\{\frac{-j\Delta}{\Sigma}\right\}, \qquad (2)$$

where Σ and Δ are the sum and difference voltages respectively as given by (1) and K is the monopulse error slope. It was found that the indicated angle became insignificant when (2) was re-computed after rotating the aperture through the initial indicated angle. Therefore, ϵ given by (2) under the above conditions is taken to be the boresight error.

Numerical Results

To illustrate the above analysis consider a tangent ogive radome of length 30λ and base diameter 10λ with constant wall thickness. The antenna has diameter 8λ and its center is 2λ above the radome base plane. The aperture has uniform sum illumination.

The wall has a dielectric constant of 3.2, loss tangent of 0.008, and half-wave length thickness at a design angle of 60^{o}. The transmission properties of the wall are shown in Figure 2.

Since boresight error is related to phase-front distortion, insight into this aberration is gained from the phase of the incident fields at the aperture. Figures 3 through 5 show the insertion phase due to the radome for rays traced directly to the aperture. The scan angle is 10^{o} and the aperture is normal to the incident rays. Figures 3 and 4 are for TE and TM polarization respectively. It is noted that these figures have even symmetry about the yz-plane, but the mean phase slope differs greatly in the z' direction. This leads to BSE with different signs in the α scan direction and no BSE in the β scan direction.

Figure 5 shows the phase front for linear polarization with 45^{o} polarization angle. No symmetry exists for this situation and there is a mean phase slope in both the x' and z' directions. This leads to BSE in both the α and β scan angles.

The polarization sensitivity seen in Figures 3 to 5 is directly attributable to the transmission properties of the wall. For the scan angle considered, the ray incidence angles range over approximately 70^{o}-85^{o}. Figure 2 shows that in this range the IPD curves have their greatest difference and their slopes also differ significantly. A wall design which minimized these differences would show much less polarization sensitivity.

BSE in the α scan direction is shown in Figure 6 for several polarizations. Greatest sensitivity to polarization is for 5^{o}-10^{o} scan angles which produce angles of incidence in the 70^{o}-85^{o} range. Little polarization effect is noted past 30^{o}, since this results in incidence angles where the IPD's are well matched. The large BSE between 15^{o} and 25^{o} is due to reflection from the interior wall which causes a large incident field component on the aperture half near the reflecting surface. Tapered aperture illumination reduces the effect of this.

Summary

A three-dimensional radome model has been presented to show the

sensitivity of BSE to the polarization of the incident field. BSE is shown to vary significantly with polarization at certain scan angles and three-dimensional plots of the wavefront over the aperture show clearly how this is related to wavefront distortion.

References

[1] G.K. Huddleston, H.L. Bassett, and J.M. Newton, "Parametric Investigation of Radome Analysis Methods," Proc. Fourteenth Symp. Electromagnetic Windows, Georgia Institute of Technology, pp. 21-27, June 1978.

[2] G. Tricoles, "Radiaton Patterns and Boresight Error of a Microwave Antenna Enclosed in an Axially Symmetric Dielectric Shell," J. Optical Soc. Amer., Vol 54, No. 9, pp. 1094-1101, Sept. 1964.

[3] R.A. Hayward, E.L. Rope, and G. Tricoles, "Accuracy of Two Methods for Numerical Analysis of Radome Electromagnetic Effects," Proc. Fourteenth Symp. Electromagnetic Windows, Georgia Institute of Technology, pp. 53-57, June 1978.

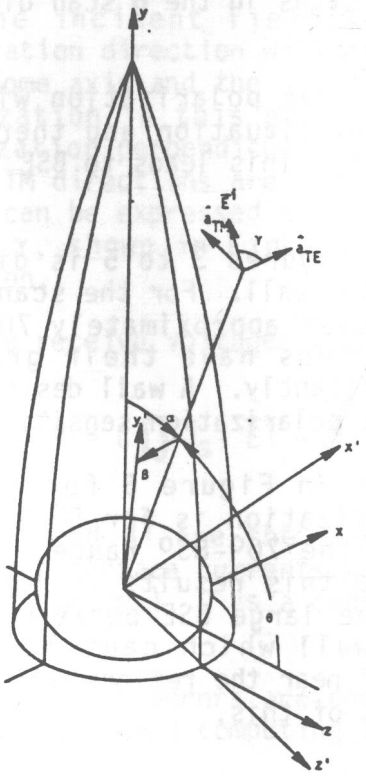

Figure 1. Outline of Tangent Ogive Radome Showing Both Scan Angles and the Polarization Angle.

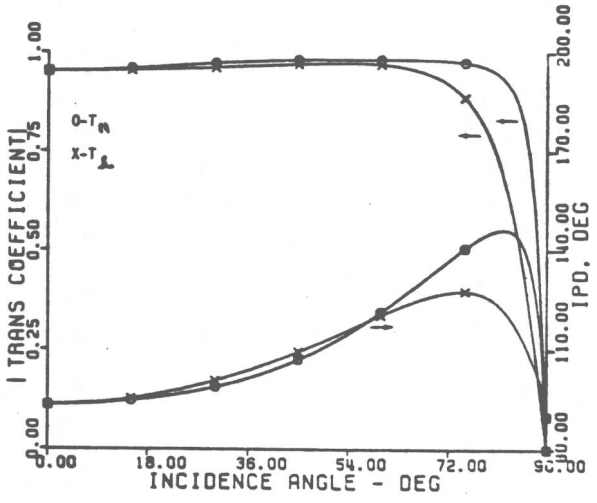

Figure 2. Transmission Coefficients of Polyimide Quartz Wall Designed for 60°.

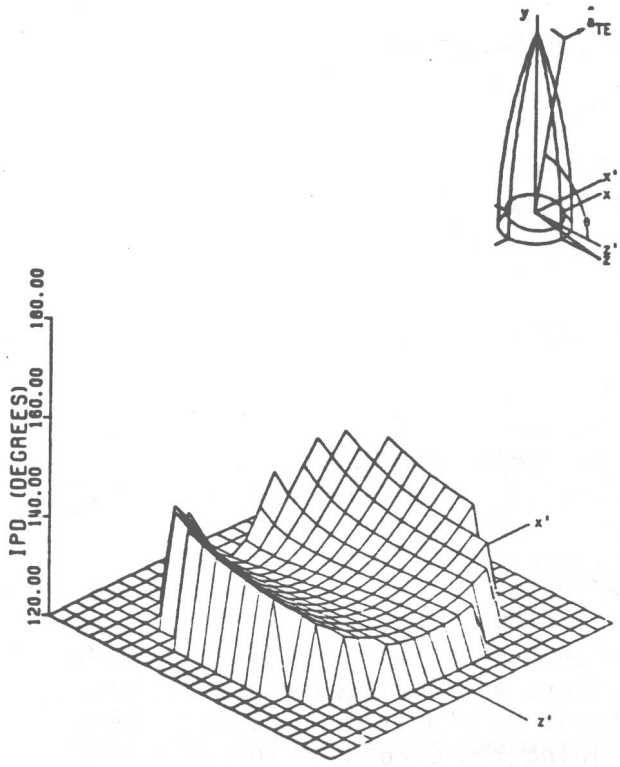

Figure 3. Insertion Phase Delay of TE Polarized Field Incident at 80° on Polyimide Quartz Radome.

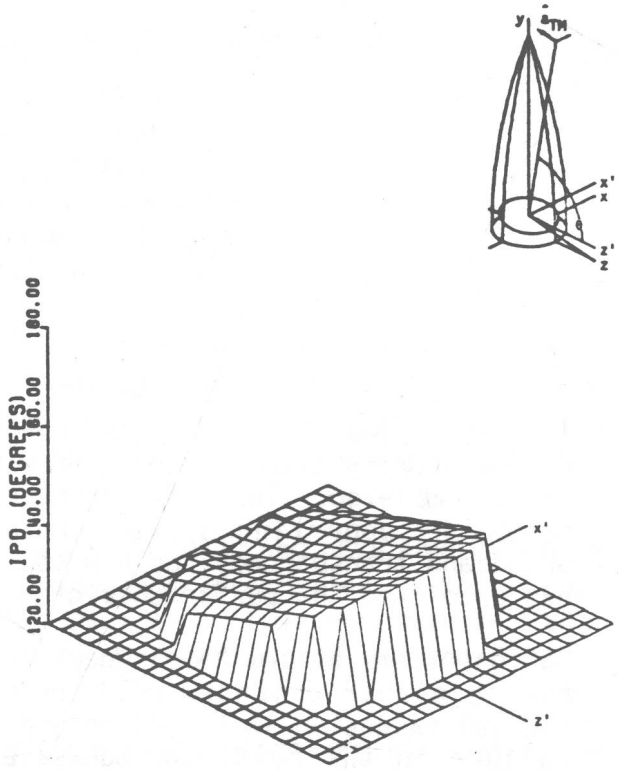

Figure 4. Insertion Phase Delay of TM Polarized Field Incident at 80° on Polyimide Quartz Radome.

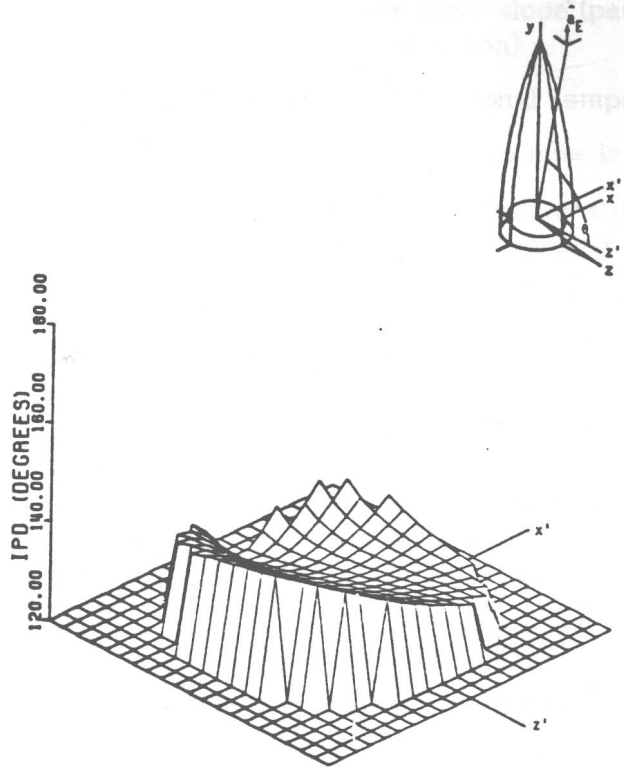

Figure 5. Insertion Phase Delay of 45° Polarized Field Incident at 80° on Polyimide Quartz Radome.

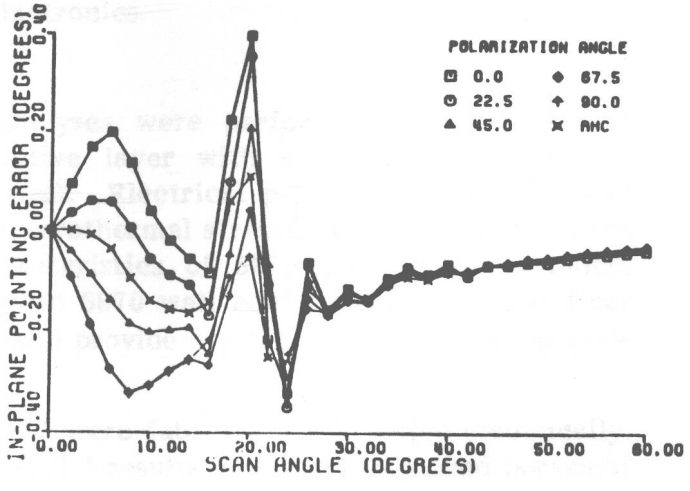

Figure 6. In-Plane Radar Pointing Error for Radome with 60° Wall Design and Various Incident Polarization.

MULTIOCTAVE SUPERSONIC RADOME WITH DUROID SKIN

Don L. Purinton
Antenna Laboratory
Texas Instruments Incorporated
P. O. Box 226015
M/S 333
Dallas, Texas 75266

An AFAL funded study for developing a supersonic high fineness ratio radome having transparency across the complete microwave spectrum is being completed. The wall structure consists of a polyimide quartz "C" sandwich supporting a thin Duroid shell. Electrical tests have shown broadband transparency for a monopulse spiral and computer simulation has predicted the performance of a large aperture single band antenna.

Hot gas tests at the Naval Weapons Center have shown that Duroid shells having planar oriented reinforcing fibers are inadequate as the large thermal expansion in the direction without reinforcement causes shear failure in the polyimide adhesive holding the Duroid to the polyimide quartz shell. A molded shell having three dimensionally oriented fibers is being prepared for testing in May 1980.

RESULTS OF A STUDY USING RT DUROID 5870 MATERIAL FOR A MISSILE RADOME

D. Brown, T. E. Fiscus, C. J. Meierbachtol
General Dynamics Electronics Division
San Diego, California

INTRODUCTION – This technical effort is the result of a recent General Dynamics Electronics Division sponsored research program. The objective of the study was to analyze several practical organic materials for use to fabricate tactical missile radomes. The Sparrow AIM-7F missile radome, used as the baseline, is currently made from Pyroceram 9606[1] glass ceramic.

Several organic materials, such as Avcoat 8029, Duroid 5650, and 5870 ablatives to be used with epoxy/glass or polyimide/quartz substrates, were investigated. A study of the ablative and rain erosion characteristics[2,3] of the ablative type materials resulted in the selection of Duroid 5870[4] to be used either in a monolithic wall or in combination with a fiberglass substrate.

The following performance characteristics improvements of an organic radome, as compared to a current Sparrow production unit, were selected as goals:

a) Increase the operating frequency bandwidth

b) Decrease the boresight error slope (particularly at the ends of the frequency band as a function of field polarization)

c) Reduce the effect of operational temperature changes on electrical performance

d) Provide improved protection to missile electronics from laser environments

e) Decrease internal radome temperatures to provide lower temperatures for the missile system antenna and processing electronics

f) Decrease unit costs

Aerothermal, mechanical, and electrical analyses were performed on radome walls configured with: 1) Duroid 5870 as an ablative layer with a quartz/polyimide substructure and 2) a monolithic Duroid 5870 wall. Electrical performance of both wall configurations are nearly equal; however, the aerothermal stresses which result from the differences in the thermal expansion characteristics of 5870 and quartz/polyimide, forced more detailed analyses of the monolithic 5870 wall configuration. Proper fiber orientation within the 5870 monolithic wall, can provide a viable design for the Sparrow type missile radome.

Several radomes made of Duroid 5870 material were fabricated and tested electrically. The lower dielectric constant of the 5870 material results in greatly improved boresight error performance when compared to the Pyroceram 9606 radome.

RADOME CONFIGURATION – The radome has a Von Karman shape with a L/D of 2.1, Figures 1 and 2. The radome is bonded to a fiberglass sleeve with radial screws for attachment to the missile. The thicknesses of the 5870 and quartz/PI wall configurations were varied as part of the electrical and aerothermal analyses. The monolithic configured radome wall is a $\lambda/2$ design with appropriate thickness variation for best electrical performance. The nose of the unit is protected by a metal tip and the exterior surface is coated with rain erosion material. The erosion coating provides rain protection to the 5870 during the air-carry phase of the missile mission. The erosion coating is a moisture-cured polyurethane.

AERODYNAMIC STRESSES – The bending, shear, and axial stresses due to aerodynamic loading were determined for the worst case missile trajectory. The radome load distribution for a 12.5° angle of attack and the resulting bending and shear loads are shown in Figure 3.

The bending moment load increases from the tip of the radome to the base, with about a three times increase between stations 9 and 16. The worst case bending stresses occur at the junction of the radome and the attachment sleeve (station 13.5) primarily due to: 1) lower mechanical properties of the radome as compared to the sleeve; and 2) largest bending loads are at the base end of the radome.

The shear load tapers toward the base of the radome; however, because of the reduction in the cross-sectional area of the radome at the transition between the radome and sleeve, the shear stresses are most severe at station 13.5.

The axial pressure load due to external pressure when the angle of attack is zero is very small and is normally considered negligible for streamline radomes.

The maximum stresses caused by the aerodynamic loads and the allowable stress for the 5870 monolithic radome wall are shown in Table 1. It can be seen that the margin of safety is substantial in all cases.

Table 1. Maximum Aerodynamic Stresses Compared to 5870 Material Allowable Stresses

STRESS TYPE	ALLOWABLE STRESS (psi)	ACTUAL STRESS (psi)
Bending	7,500	698
Shear	7,500	193
Axial	10,000	436

AEROTHERMAL STRESSES – The most significant thermal-induced effect on the radome configurations are stresses caused by the difference in the temperature between the outer and inner surfaces. The outside of the radome tends to elongate because of the

increase in temperature while the internal surface does not elongate as rapidly because of the lower surface temperature.

The worst case missile trajectory for radome thermal stresses has been used for the thermal analysis. The maximum outer, mid, and inner surface temperatures of the Von Karman shaped radome made from Pyroceram 9606 and Duroid 5870 are shown in Figure 4. The mid and inner surface temperatures of the 5870 radome are lower than the 9606 radome because of the lower thermal conductivity of 5870. The inner surface temperature of the 5870 radome is 370° F which is the result of sustained air carry on board the launching aircraft.

The most exact solution of thermal stresses of composite type materials requires a finite element model because of the orthotropic properties of these materials. Such a model can accommodate changes in material properties, magnitude of loads/stresses, wall thickness variations and thermal distributions all as a function of position on the radome.

The radome model configurations analyzed using a finite element model were: 1) Duroid 5870 outer surface bonded to a substrate of quartz/polyimide; and 2) Duroid 5870 alone. The base portion of both configurations (attachment sleeve) was given the properties of glass reinforced phenolic. The substrate thickness was varied as 0, 1/8, 1/4, and 1/2 of the overall radome thickness. The 5870 glass fiber orientation was also varied from the radial/tagential (normal to radome wall and circumferential) directions to the longitudinal/tangential (parallel to radome wall lengthwise and circumferential) directions.

The thermal stress for the two wall configurations and fiber orientations are shown in Figure 5. The radial/tangential fiber orientation in the 5870 material coupled with the 5870 outer shell and quartz/PI substrate show that the longitudinal thermal stresses at the outer surface exceed the allowable stress of the 5870 material. The external tangential stresses are well within the allowable values because the fiber orientation is radial/tangential in the 5870 material. The monolithic 5870 wall configured with the longitudinal/tangential fiber orientation shows that both the longitudinal and tangential stresses are well within the 5870 material properties allowable values.

Numerous thermal stress computer runs were made for combinations of substrate thicknesses and 5870 fiber orientations; however, none of the results predicted a successful combination. Hence, the monolithic 5870 wall with the longitudinal/tangential fiber orientation was selected as the design that would satisfy the requirements.

ELECTRICAL PERFORMANCE – The 5870 monolithic radome assembly (Figure 2) was electrically tuned for optimum boresight error performance. The boresight error characteristics of this radome and a current production 9606 radome were measured at the low and high ends of the operating frequency band. A total of 108 measurements were made at each frequency consisting of 36 radome and system antenna roll positions (0° to 175° in 5° increments) and three field polarizations at each roll position, i.e. colinear and ±45° cross polarization.

The data was digitized and computer analyzed to determine the slope of the boresight error components, inplane and crossplane. The percent occurrence of each component of error slope for 108 measurements at both the high and low frequencies are shown in Figure 6. The 5870 radome has smaller error slope magnitudes for both the inplane and

crossplane cases at the low and high frequencies. The significant improvement is the low frequency crossplane data where the magnitude of the slope is about one-half of the 9606 radome. The major contributor to the crossplane error slope at the low frequency is the $\pm 45^{\circ}$ cross polarization data. The bandwidth characteristics of the 5870 radome are sufficiently larger than the 9606 radome to allow a thickness increase for improving the low frequency crossplane error slope.

CONCLUSIONS – The monolithic Duroid 5870 wall configuration will meet the aero-thermal requirements of the Sparrow AIM-7F missile radome. The thermal conductivity of the material provides improved thermal and laser protection (as compared to Pyroceram 9606) to the electronics housed within the radome.

The overall electrical performance of the radome is better than the 9606 radome; in particular the magnitude of the crossplane error for cross polarization conditions are greatly improved at the low frequency. The effect of ablation/erosion of the exterior surface of the radome on electrical performance is not known. Analyses indicates that a small amount of ablation can be expected in the nose region of the radome. The change in electrical performance of the radome can only accurately be determined by testing. Ablation and rain erosion tests are planned in the near future.

Processing costs of a Sparrow type radome made from Duroid 5870 are presently high because of the low quantity being manufactured. Investigations show that unit production costs should be lower than Pyroceram 9606 primarily due to the lower molding and finishing time required for the Teflon based 5870 material.

REFERENCES

1. Corning Glass Works Material Handbook, "Pyroceram Brand Glass Ceramics," Seventh Edition, 1965.
2. W. G. Burleson, "Evaluation of Aerothermal Ablation and Rain Erosion Results for Plastic Radome Materials Tested on Sleds at Mach 5," U.S. Army Missile Command, Redstone Arsenal, Alabama, Technical Report No. RL-77-3.
3. G. F. Schmitt, Jr., "Supersonic Rain Erosion Behavior of Ablative Fluorocarbon Plastic Radome Materials," Proceedings of Fourteenth Symposium on Electromagnetic Windoes, Georgia Institute of Technology, June 1978.
4. "RT Duroid 5870 Data Sheet," Rogers Corporation, Engineered Products Group, Lithonia, Georgia.